



Chemical modification of monensin as a source of potent antiplasmodial agents

Michał Sulik^{a,1}, Eyob A. Workneh^{b,1}, Sofia Santana^b, Bárbara Teixeira^b, Miguel Prudêncio^{b,c}, Jan Janczak^d, Adam Huczynski^{a,*}

^a Department of Medical Chemistry, Faculty of Chemistry, Adam Mickiewicz University, Uniwersytetu Poznańskiego 8, 61-614 Poznań, Poland

^b GIMM - Gulbenkian Institute for Molecular Medicine, Avenida Prof. Egas Moniz, 1649-035 Lisboa, Portugal

^c Faculdade de Medicina da Universidade de Lisboa, Av. Prof. Egas Moniz MB, 1649-028 Lisboa, Portugal

^d Institute of Low Temperature and Structure Research, Polish Academy of Sciences, Okólna 2, Wrocław 50-422, Poland

ARTICLE INFO

Keywords:

Ionophores
Plasmodium berghei
Antiplasmodial activity
Malaria
Crystal structure

ABSTRACT

Malaria remains a significant public health issue and one of the leading causes of child mortality worldwide. Due to the growing problem of drug resistance, new modes of fighting the disease are searched for. In this context, ionophore antibiotics, natural compounds with high potential for combating parasitic diseases, deserve special attention. The primary representative of such compounds, monensin (MON), demonstrates exceptionally high antiplasmodial activity. In this work, the C26-amino derivative of MON was used as a convenient substrate for the synthesis of its acyl analogues, such as amides and urea. All derivatives exhibited strong activity against the hepatic stage of *Plasmodium berghei* infection *in vitro*, which exceeded that shown by the reference drug primaquine. The IC₅₀ value for MON *O*-phenyl urethane (**8**) was less than 1 nM.

1. Introduction

According to WHO data, in 2023, malaria caused the death of nearly 600,000 people, making it the deadliest parasitic disease in the modern world.¹ Malaria is caused by *Plasmodium* parasites transmitted in their sporozoite form by infected female *Anopheles* mosquitoes.^{1,2} After injection into their mammalian host during an infected mosquito bite, sporozoites asymptotically infect and replicate inside hepatocytes, generating thousands of hepatic merozoites. Following their release into the bloodstream, merozoites cyclically infect erythrocytes causing the symptoms of malaria. These include fever and headache, but may progress to cause severe disease, or even death.^{1,3,4} The most important malaria control strategies involve vector control, the introduction of the RTS,S/AS01, and the R21/Matrix-M malaria vaccines, and chemotherapies.^{1,5} Several medicines are currently available to treat malaria (e.g. chloroquine, primaquine, and artemisinin combination therapies), but due to the growing problem of drug resistance, the quest for new

antimalarial drug candidates is highly desirable.^{1,2,6}

Among many natural compounds with high biological activity, ionophore antibiotics have merited particular attention, as they exhibit a wide range of antiparasitic activities.⁷ The main representative of this group of compounds is monensin (MON, Fig. 1), which is successfully used in veterinary practice as an animal feed additive that prevents coccidiosis (Coxidin®).⁸ The high antimicrobial activity of MON results from its natural ability to coordinate metal cations and transfer them across biological membranes.^{7,9} This phenomenon leads to the disturbance of the intracellular pH and ion concentration gradient, which leads to mitochondrial damage, vacuolization, and eventually cell death.^{7,9} In addition to its anticoccidial activity, MON has proven its potential in combating parasites causing diseases such as trypanosomiasis, leishmaniasis, toxoplasmosis, and malaria.^{7,10-14} Several studies aimed at the chemical modification of MON skeleton to obtain compounds with enhanced biological activity have been reported.¹⁵⁻¹⁷ They concerned the anticancer and antibacterial properties of this type of

Abbreviations: aq, aqueous solution; DBU, 1,8-diazabicyclo[5.4.0]undec-7-ene; DMF, dimethylformamide; DMSO, dimethyl sulfoxide; HRMS, high resolution mass spectrometry; Huh7, human hepatoma cell line; IC₅₀, half maximal inhibitory concentration; MON, monensin A; NMR, nuclear magnetic resonance spectroscopy; rt, room temperature; SAR, structure-activity relationship; TEA, triethylamine; TPP⁺, triphenylphosphonium cation; TsCl, 4-toluenesulfonyl chloride; WHO, World Health Organization.

* Corresponding author.

E-mail address: adhucz@amu.edu.pl (A. Huczynski).

¹ These authors contributed equally to this work.

<https://doi.org/10.1016/j.bmc.2025.118177>

Received 23 January 2025; Received in revised form 26 March 2025; Accepted 26 March 2025

Available online 30 March 2025

0968-0896/© 2025 Elsevier Ltd. All rights reserved, including those for text and data mining, AI training, and similar technologies.

derivatives.^{16–18} Although reports on the antiparasitic activity of **MON** analogues are still limited, some studies have shown that rational modification of its structure can lead to the derivatives with higher antiparasitic potential than the unmodified ionophore.^{7,13,14,17–19} **MON** and some of its analogues have been shown to display potent activity against malaria parasites. Among them, C26-modified analogues, such as tosylate or carbonate, exhibited *in vitro* activity against *P. falciparum* with IC₅₀ values of 1.52 and 1.08 nM, respectively, exceeding the activity of the starting compound (Fig. 1).^{7,13,14} Nevertheless, the chemical modification of **MON** to find new antiplasmodial derivatives remains a very promising, and still underexplored, research direction.

2. Results and discussion

2.1. Design strategy

As mentioned above, the antimicrobial activity of ionophore antibiotics results from their natural ability to coordinate metal cations and transport them across biological membranes.^{7,9} This process occurs via electroneutral transport with deprotonation of the carboxyl group or electrogenic transport without deprotonation of the carboxyl group, without or with a change in the transmembrane potential, respectively.^{20,21} This means that modification of group C26 of **MON** is a promising approach to obtain its bioactive analogues, as it does not hinder the carboxyl group from participating in the ion exchange mechanism. However, it has also been shown that ionophores with a modified carboxyl group can perform a third type of transport, known as biomimetic transport.^{20,21}

Chemical modification of C1 carboxyl group of **MON** is a well-known and frequently used method for the synthesis of numerous analogues of this ionophore.^{9,15} The molecule's C26 hydroxyl group has also often been modified, but no method has been reported for converting it into another functional group as a convenient lead structure. Thus, C26 derivatives of **MON** were limited to its esters, ethers, or *O*-urethanes.^{9,15} However, our team has recently developed the first scalable, efficient, and simple method for obtaining **MON**'s C26 amine.²² The reaction consists of tosylation and subsequent azidation of C26 hydroxyl group. The obtained azide was then reduced to amine using hydrogen in the presence of palladium on carbon (compound **2**, Scheme 1).²²

2.2. Chemistry

Having access to an amine precursor, it is possible to synthesize numerous analogues, such as amides or ureas. Therefore, in this paper, we present the synthesis and antimalarial activity of a narrow library of compounds, which illustrates the potential for developing different groups of new **MON** derivatives. We chose to synthesize aromatic analogues as representatives of each group of derivatives because previous

studies have shown their antimicrobial potential.¹⁷ Acylated derivatives of **2** include its benzoyl amide (compound **3**) and phenyl urea (compound **4**). In addition, an amide conjugate of **MON** with a triphenylphosphonium cation (TPP⁺, compound **5**) was also obtained (Scheme 1). This chemical moiety is naturally directed to the mitochondria due to their highly negative membrane potential.^{23,24}

It is worth noting that several reports have suggested that *Plasmodium* mitochondria are important therapeutic targets.^{25,26} Furthermore, to extend the knowledge about the antimalarial activity of C1 derivatives of **MON**, its benzyl ester (compound **7**) and ester conjugate with TPP⁺ (compound **6**) were also synthesized (Scheme 1). For comparative purposes, the resynthesis of **MON** *O*-phenyl urethane (compound **8**) was performed, as this compound showed high antimicrobial activity in previous studies.¹⁷

The purity and structure of the newly synthesized and resynthesized **MON** derivatives (**2–8**) were determined using spectroscopic (¹H NMR, ¹³C NMR, ³¹P NMR) and spectrometric (HRMS) methods (see Supplementary Information). In the ¹³C NMR spectra of **MON** C26-analogues (compounds **3**, **4**, **5**, and **8**), the signals of the highest analytical significance were assigned to the carboxyl group and appeared in the range of 177.4–184.2 ppm. For C1-esters of **MON** (compounds **6**, and **7**), the signals from the ester group appeared in the narrow range of 175.2–176.0 ppm. With respect to the newly introduced carbonyl group at position C26 of **MON** (compounds **3**, **4**, **5**, and **8**), respective signals from the amide/urethane/urea group appeared in the range of 154.7–174.1 ppm. The HRMS analysis confirmed the formation of the intended products, with [M + Na]⁺ as the main peak (100 % intensity) for compounds **3**, **4**, **7**, and **8**, and [M]⁺ for compounds **5**, and **6**. The NMR spectra of all obtained **MON** derivatives, are included in the Supplementary material (Figs. S1–S16).

X-ray diffraction analysis was employed to confirm and explain the structure of **MON** derivatives as well as to extract possible structure–activity relationships (SAR). Therefore, two of the C26 derivatives obtained – **MON** phenyl urea (compound **4**) and **MON** amide conjugate with TPP⁺ (compound **5**) as their sodium salts were characterized using the X-ray single crystal diffraction method. Detailed crystal data, refinement parameters and experimental details for both molecules are presented in Table S1 and Figs. S17–S18 (Supplementary material). Single crystals of compounds **4** and **5** were grown by crystallization in acetonitrile solution. The urea derivative crystallized in the non-centrosymmetric space group *R*3:H of the trigonal system, as a solvate with water molecules, while the amide derivative crystallized in the non-centrosymmetric space group *P*2₁2₁2₁ of the orthorhombic system with bromide as counterions and as a solvate with water molecule. The asymmetric unit of both compounds are illustrated in Fig. 2.

Both molecules form complexes with the sodium cation, with the C26 substituent not involved in the coordination process. The pseudo-cyclic structure is stabilized by several hydrogen bonds, whose exact geometry

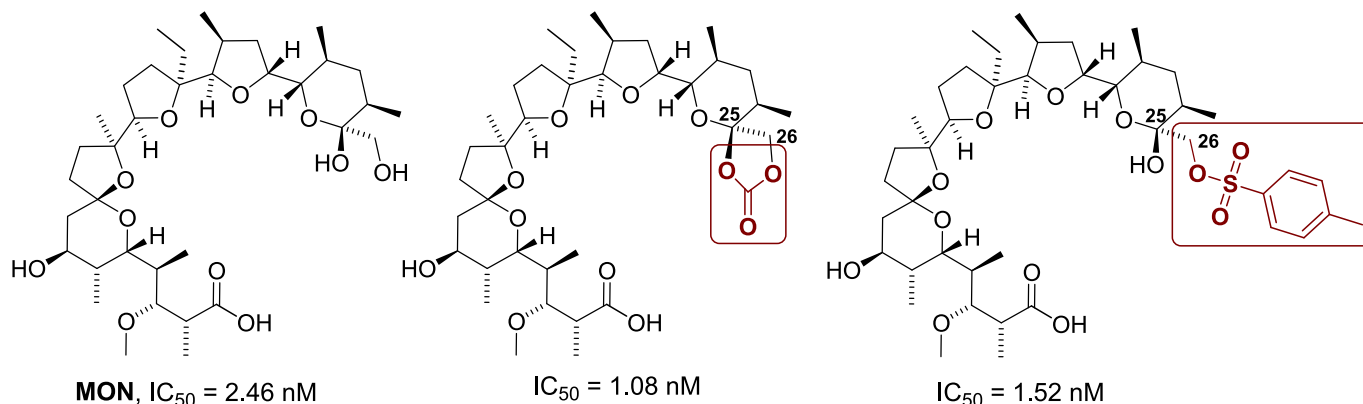
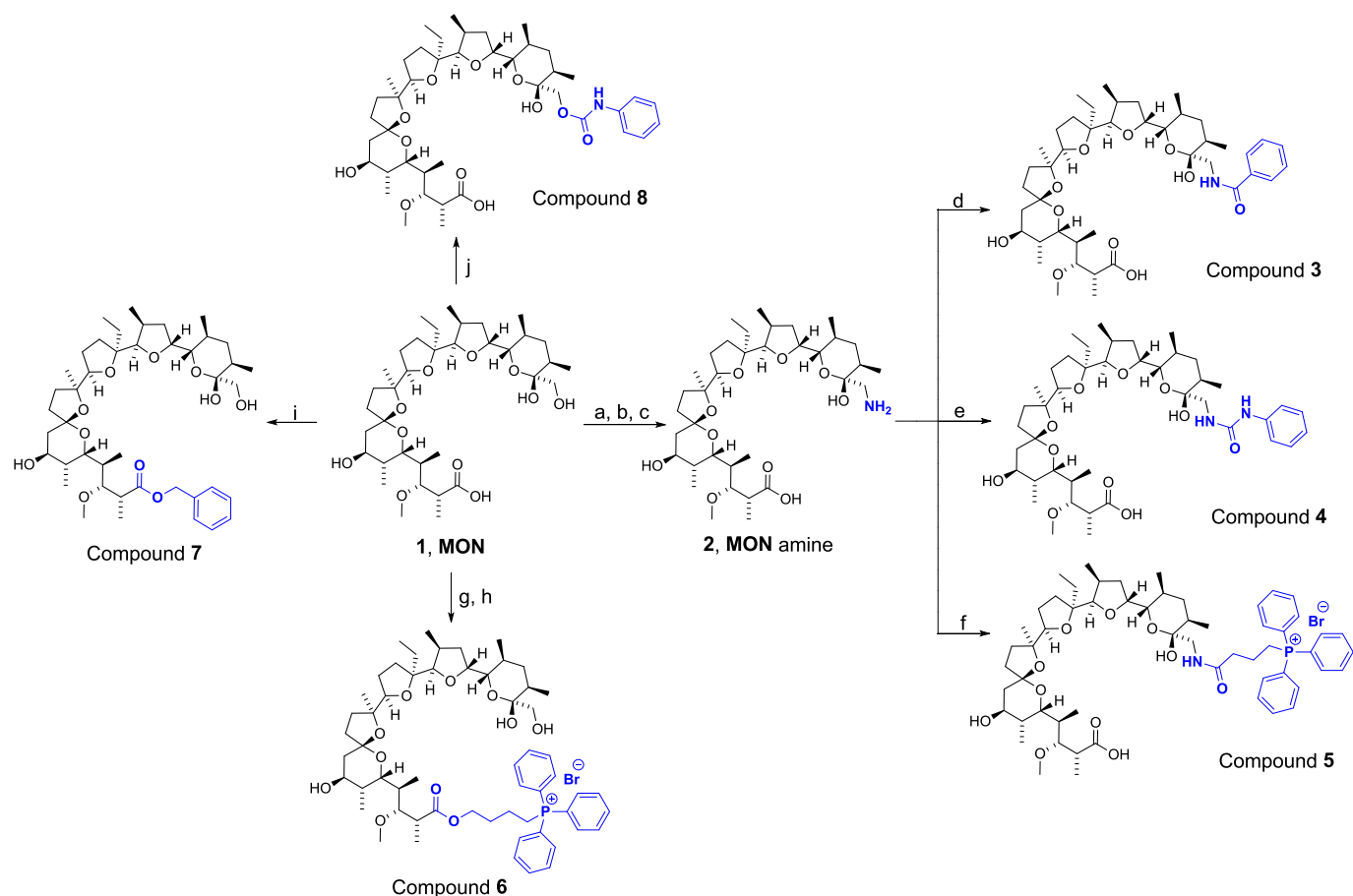


Fig. 1. *In vitro* activity of **MON** and its C26-derivatives against *P. falciparum*.



Scheme 1. Synthesis of MON aromatic derivatives. *Reagents and conditions:* (a) TsCl, Na₂CO_{3(aq)}, toluene, rt, 72 h; (b) NaN₃, DMSO, rt, 72 h; (c) H₂, Pd/C, MeOH, rt, 72 h; (d) benzoyl chloride, TEA, CH₂Cl₂, 0 °C to rt, 24 h; (e) phenyl isocyanate, toluene, rt, 72 h; (f) (3-carboxypropyl)triphenylphosphonium bromide, ethyl chloroformate, TEA, DMF, -5 °C to rt, 24 h; (g) 1,4-dibromobutane, DBU, toluene, 90 °C, 24 h; (h) triphenylphosphine, CH₃CN, reflux, 72 h; (i) benzyl bromide, DBU, toluene, 90 °C, 24 h; (j) phenyl isocyanate, toluene, rt, 14 days.

is described in the [Supplementary material \(Tables S2–S3\)](#). In the case of **4**, we can see that the urea moiety is involved in the formation of hydrogen bonds N1—H1...O1 and N2—H2N...O1. The structure is additionally stabilized by the hydrogen bonds formed by water molecules acting as donors ([Fig. 2a](#)). With respect to compound **5**, the only hydrogen bond formed between the atoms constituting its molecule is the O1—H1A...O10. The formation of the remaining hydrogen bonds involves the bromide anion as an acceptor or a water molecule as a donor ([Fig. 2b](#)).

A comparison of the crystal structure of urea **4** with the previously published crystal structures of urethane **8** leads to several interesting observations ([Fig. 3](#)).²⁷ Firstly, the nitrogen atom of the urethane group in compound **8**, similarly to the urea group of compound **4**, participates in the formation of a hydrogen bond stabilizing the pseudo-cyclic structure of the compound (N1—H1...O1).²⁷ Secondly, a formation of hydrogen bond O10—H10O...O2 is observed for both compounds.²⁷ Thirdly, although the hydroxyl group O4—H4O acts as the hydrogen bond donor for both compounds, in the case of urea **4**, the role of the acceptor is assumed by the oxygen atom O10 of the hydroxyl group, whereas in the structure of urethane **8**, the role of the acceptor is played by the oxygen atom O2 of the carboxyl group ([Fig. 3](#)).²⁷ Despite very similar structural features, both compounds crystallize in different space groups, with urea **4** crystallizing in space group R3:H of the trigonal system, and urethane **8** crystallizing in space group P1 of the triclinic system.²⁷

2.3. *In vitro* antiplasmodial activity

To evaluate the antiparasitic potential of MON derivatives, all six analogues (compounds **3–8**), the MON parental compound (compound **1**), and primaquine, employed as a reference, were screened *in vitro* for their antiplasmodial activity against the hepatic stage of *P. berghei* infection ([Fig. 4](#), [Table 1](#)).

MON (compound **1**) and its derivatives (**3**, **4**, **5**, **6**, **7**, and **8**) exhibited strong activity against the hepatic stage of *P. berghei* infection *in vitro*, which exceeded that shown by primaquine – a commonly used drug in treating malaria. Among these derivatives, compounds **8** (IC₅₀ = 0.0007 μM) and **4** (IC₅₀ = 0.0029 μM) displayed the highest potency, followed by MON (IC₅₀ = 0.0055 μM) and derivative **3** (IC₅₀ = 0.0064 μM), both showing comparable activity ([Table 1](#)). Derivative **5** (IC₅₀ = 1.489 μM) had the lowest activity from among the compounds tested, whilst derivatives **6** (IC₅₀ = 0.6233 μM) and **7** (IC₅₀ = 0.0816 μM) displayed intermediate potency hepatic parasites ([Table 1](#)). In addition to nanomolar IC₅₀ values against *P. berghei*, the CC₅₀ values of most compounds against the Huh7 cell line remain in the micromolar range. Compounds **3** and **4** exhibit high selectivity (SI > 1300), although not as high as that observed for the unmodified MON (SI = 3181.8). It is important to highlight that compound **8**, despite having the lowest CC₅₀ value among the tested compounds, remains the most selective compound in the entire series of analogs studied, due to its extraordinarily high antimalarial activity (SI = 4428.6).

Concerning the SAR (structure–activity relationship) analysis, it should be emphasized that the derivatives showing higher activity than

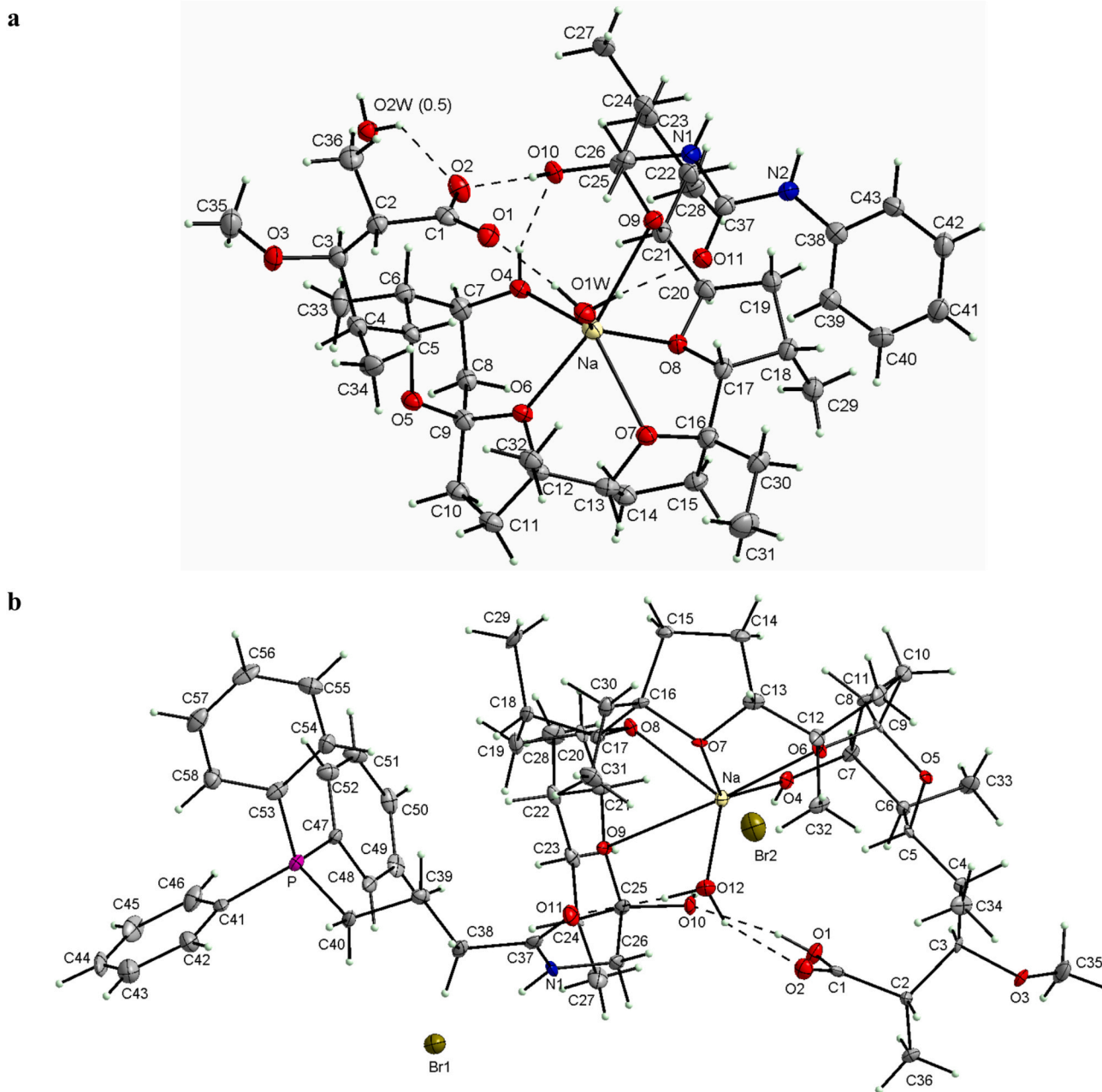


Fig. 2. The crystal structure of: (a) sodium salt of C-26 phenyl urea monensin **4**, (b) sodium salt of C-26 monensin conjugate with TPP⁺ **5**. Ellipsoids are at the 50 % probability level.

unmodified **MON** belong to the group of its C26-analogues (compounds **4** and **8**). Amide **3** also exhibited high antimalarial activity, which was similar to that of **MON**. We can see that chemical modification of position C26 of **MON** gives better results in the context of antimalarial activity, than modification of its C1 position. An exception is compound **5**, which is a C26-conjugate of **MON** with TPP⁺. This compound's decreased activity is probably due to its high steric hindrance, which impedes effective penetration into the parasite cells. Ester compounds **6** and **7** also show lower biological activity than **MON**. This may suggest that potent antimalarial derivatives of **MON** must contain an unhindered carboxyl group, which will enable effective ion transport via an electrogenic or electroneutral mechanism. It is worth noting that the derivatives obtained through chemical modification of the C26 position of **MON** (except for compound **5**) exhibit high selectivity indices (SI > 1300) which means they preferentially target parasite cells over reference Huh7 cell line. Of particular distinction is compound **8**, which is

not only the most active compound in the entire series (with an IC₅₀ value approximately 8 times lower than that of **MON**) but also the most selective one (SI > 4000).

3. Conclusions

In summary, in this work, we describe the possibility of using the C26-aminomonensin (compound **2**) as a convenient starting substrate for the synthesis of various analogues, such as amides or ureas (compounds **3–5**). This significantly contributes to the search for new, highly bioactive analogues of this ionophore. For comparative purposes, C1 ester derivatives of **MON** (compounds **6**, and **7**) and its C26-O-phenyl urethane (compound **8**) were also obtained. Compounds **4** and **5** were obtained in crystalline form, which enabled sXRD analysis to be performed. Both molecules form complexes with the sodium cation and occur in a pseudo-cyclic structure, which is stabilized by numerous

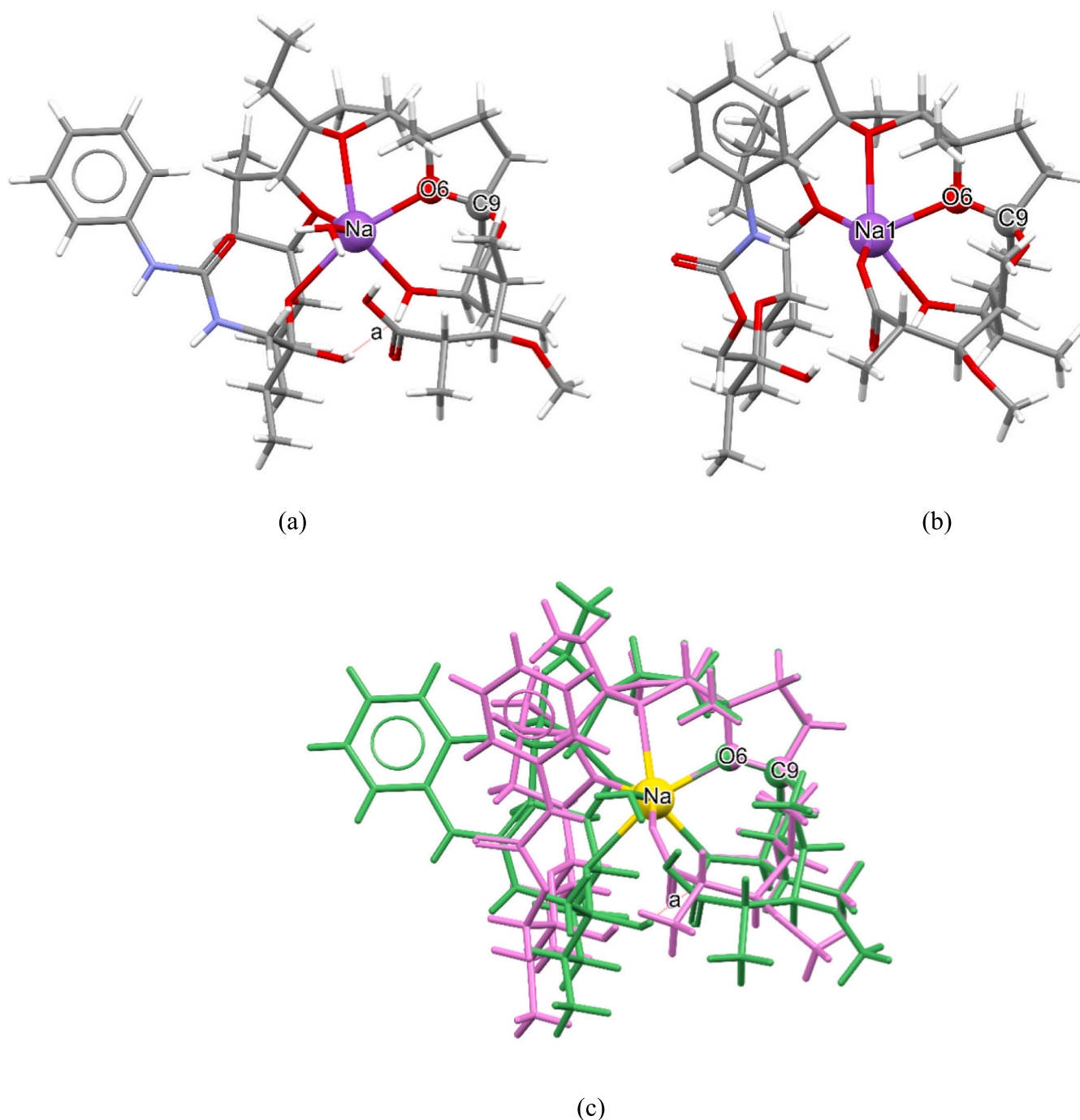


Fig. 3. Comparison of the conformations of monensin sodium salts in crystals: (a) urea **4**, (b) urethane **8** and (c) overlap **4** (green) and **8** (pink), atoms Na, O6 and C9 overlap. Monensin A phenylurethane sodium salt **8** was reproduced using data downloaded from the Cambridge Crystallographic Data Centre CCDC: 778665. (For interpretation of the references to color in this figure legend, the reader is referred to the web version of this article.)

hydrogen bonds. The substituent at C26 is not involved in the coordination process. In addition, **MON** and its aromatic derivatives (**3–8**) were screened *in vitro* for their antiparasitodal activity against the hepatic stage of *P. berghei* infection. It is worth noting that these compounds showed higher biological activity than primaquine used as a reference. Most derivatives showed activity at the nanomolar level, which, in the case of compounds **4** and **8**, even exceeded that of unmodified **MON**. Furthermore, many of the obtained compounds demonstrated high selectivity, meaning they preferentially target parasite cells over the reference Huh7 cell line. The selectivity index for compound **8** exceeded a value of 4000, making it not only more active but also more selective than the unmodified ionophore. These results

underscore the strong antiparasitic potential of **MON** and its derivatives, supporting their development as promising candidates for discovery of new antimalarial drugs.

4. Experimental section

4.1. General procedures

All reagents were purchased from two sources – Merck or Trimen Chemicals S.A., and used without further purification. Deuterated solvents for NMR analysis (CDCl_3 , CD_2Cl_2 , CD_3OH , and CD_3CN) were stored over 3 Å molecular sieves for several days. Reaction mixtures

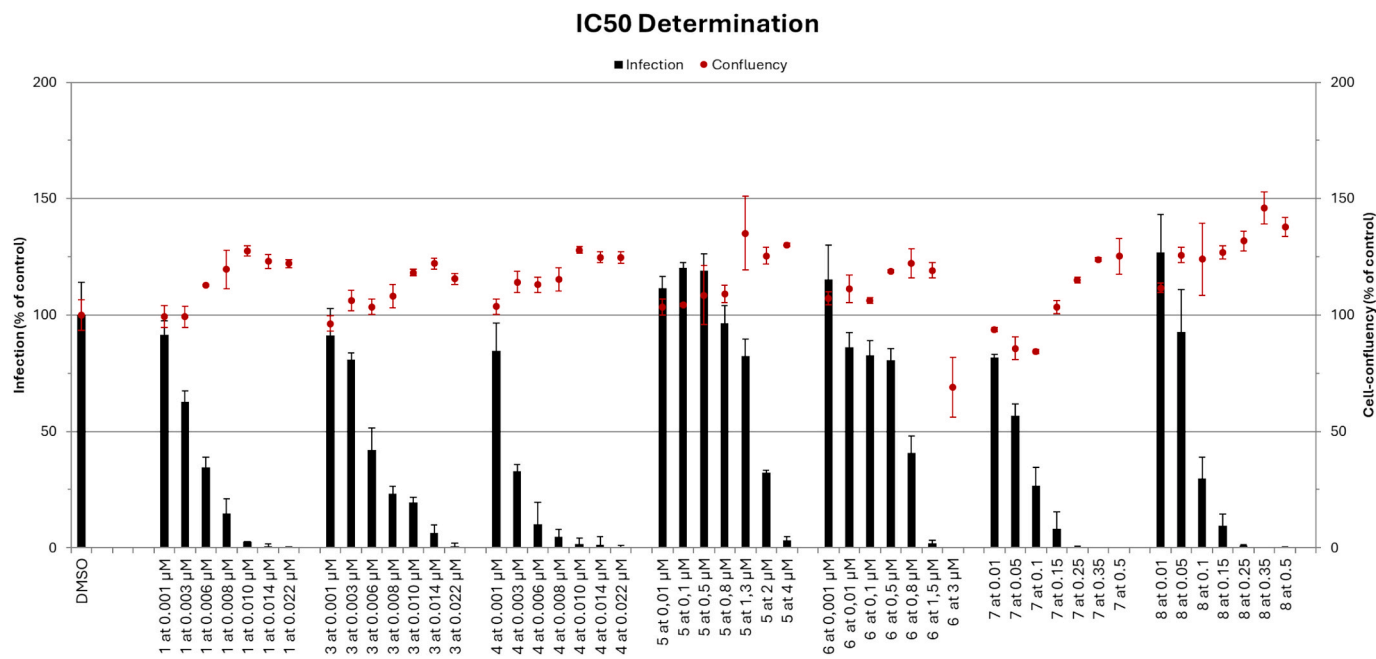


Fig. 4. Dose-dependent response of MON (compound 1), and its derivatives 3, 4, 5, 6, 7, and 8, against the hepatic stage of *P. berghei* infection. Total parasite load (infection scale, bars) and cell viability (cell confluency scale, dots) are shown. Calculated IC₅₀ values are presented in Table 1.

Table 1

IC₅₀, CC₅₀ and SI values of MON, its derivatives and primaquine against the hepatic stage of *P. berghei* infection and Huh7 cells.

	Antiplasmodial activity	Cytotoxicity	Selectivity
No.	IC ₅₀ (nM) ^a	CC ₅₀ (nM) ^a	SI ^b
monensin 1	5.5 ± 1.4	17500 ± 5700	3181.8
3	6.4 ± 1.0	8400 ± 1900	1312.5
4	2.9 ± 1.0	4200 ± 400	1448.3
5	1489 ± 162.6	75300 ± 10100	50.6
6	623.3 ± 183.0	5800 ± 300	9.3
7	81.6 ± 18.4	31300 ± 7400	383.6
8	0.7 ± 0.004	3100 ± 200	4428.6
Primaquine	8428 ± 3384	138600 ± 25400	16.4

^a Data shown are mean values ± SD of two or three independent experiments.

^b SI (selectivity index) was calculated using the formula: SI = CC₅₀ (nM)/IC₅₀ (nM).

were stirred using Teflon-coated magnetic stir bars and were monitored by thin layer chromatography (TLC) using aluminum-backed plates (Merck 60 F₂₅₄). TLC plates were visualized by UV-light (254 nm), followed by treatment with phosphomolybdic acid (PMA) (5 % in absolute ethanol) and gentle heating. Products of the reactions were purified using CombiFlash® Rf + Lumen Flash Chromatography System (Teledyne Isco) with integrated ELS and UV detectors. All solvents used in flash chromatography were of HPLC grade (Merck) and were used as received. Solvents were removed using a rotary evaporator.

NMR spectra were recorded on a Varian 400 (¹H NMR at 400 MHz, ¹³C NMR at 101 MHz, and ³¹P 162 MHz) or Bruker AvanceNEO 600 (¹H NMR at 600 MHz and ¹³C NMR at 151 MHz) magnetic resonance spectrometer. ¹H NMR spectra are reported in chemical shifts downfield from TMS using the respective residual solvent peak as internal standard (CDCl₃ δ 7.26 ppm; CD₂Cl₂ δ 5.32 ppm; CD₃OD δ 3.31 ppm; CD₃CN δ 1.94 ppm). ¹H NMR spectra are reported as follows: chemical shift (δ, ppm), multiplicity (s = singlet, d = doublet, t = triplet, p = quintet, dd = doublet of doublets, dt = doublet of triplets, td = triplet of doublets, tt = triplet of triplets, dq = doublets of quartets, ddd = doublet of doublets of doublets, m = multiplet), coupling constant(s) in Hz, and integration. Significant peaks are reported within the overlapping ~2.00–0.50 ppm region of the ¹H NMR spectra. ¹³C NMR spectra are reported in chemical

shifts downfield from TMS using the respective residual solvent peak as internal standard (CDCl₃ δ 77.16 ppm; CD₂Cl₂ δ 53.84 ppm; CD₃OD δ 49.00 ppm; CD₃CN δ 1.32 ppm). ³¹P NMR spectra are reported in chemical shifts. Line broadening parameters were 0.5 or 1.0 Hz, while the error of chemical shift value was 0.1 ppm.

Electrospray ionization high resolution mass spectra (ESI-HRMS) were recorded on a QTOF (Impact HD, Bruker Daltonics or Bruker micrOTOF-q) mass spectrometer in the positive ion detection mode. Samples were prepared in dry acetonitrile. The mass range for ESI experiments was from *m/z* = 400 to *m/z* = 1350 or to *m/z* = 1000.

4.2. Synthesis

4.2.1. Isolation of MON

The sodium salt of MON was isolated from commercially available veterinary premix – Coxidin®, as previously described.¹⁶ The obtained sodium salt of MON was then extracted with a solution of sulfuric acid (pH = 1), giving MON ready for further synthesis.

4.2.2. Synthesis of MON amine (compound 2)

To a solution of MON (11.0 g, 16.39 mmol, 1.0 equiv.) in toluene (120 mL) upon stirring, a solution of 0.1 M Na₂CO₃ was added (150 mL). After that, tosyl chloride (9.37 g, 49.18 mmol, 3.0 equiv.) was added to the resulting mixture in one portion. The resulting solution was stirred at room temperature for the next 72 h. The reaction mixture was then transferred to a separatory funnel and extracted with 0.1 M Na₂CO₃ solution and brine. After that, the organic layer was concentrated under reduced pressure, and directed subsequently to the next stage of the process. The excess of sodium azide (3.19 g, 49.09 mmol, 3.0 equiv.) was dissolved in 30 mL of DMSO (complete conversion of MON to tosylate was assumed). The solution of crude tosylate dissolved in 20 mL of DMSO was then added to the mixture. The resulting solution was stirred at room temperature for the next 72 h. The mixture was then diluted with large amount of water (over 300 mL) and extracted several times with methylene chloride. This step can be dangerous due to the possibility of an explosion as a result of the reaction between sodium azide and the chlorinated solvent, so the sequence of operations must be strictly followed. Alternatively, azide can be extracted from the aqueous phase into the ethyl acetate phase. Purification on silica gel using the

CombiFlash system (0 → 40 % EtOAc/*n*-hexane) gave the pure product as a clear oil. The oil was diluted in *n*-pentane and evaporated to dryness three times to form an amorphous solid, with an isolated yield of 62 % (7.10 g). Under a nitrogen atmosphere, to a solution of obtained azide (2.0 g, 2.87 mmol, 1.0 equiv.) in methanol upon stirring, the catalytic amount of palladium on carbon (Pd/C) was added. Then, a hydrogen-filled balloon was connected to the system. The reaction was continued until the azide was completely consumed (TLC and ESI-MS control), replacing the hydrogen balloon if necessary (typically 72 h). After this time, the reaction mixture was filtered through celite to remove Pd/C, and concentrated under reduced pressure. Purification on silica gel using the CombiFlash system (0 → 30 % MeOH/CHCl₃) gave the pure product as a clear oil. The oil was diluted in *n*-pentane and evaporated to dryness three times to form an amorphous solid, with an isolated yield of 63 % (1.22 g), a single spot by TLC; stains green with PMA. The spectroscopic data were in agreement with previously published data.²²

4.2.3. Synthesis of C26-benzoyl amide of MON (compound 3)

MON amine (compound 2, 135 mg, 0.20 mmol, 1.0 equiv.) was dissolved in CH₂Cl₂ (10 mL) and the solution was cooled on an ice bath. Triethylamine (61 mg, 0.60 mmol, 3.0 equiv.) was added dropwise to the reaction mixture, and after that, benzoyl chloride (34 mg, 0.24 mmol, 1.2 equiv.) was added dropwise. After 24 h, the reaction mixture was concentrated on a rotary evaporator *in vacuo*. Purification on silica gel using the CombiFlash system (0 %→100 % EtOAc/hexane) gave the pure amide 3 as a clear oil. After twice evaporation to dryness with *n*-pentane, the oily product was completely converted into white amorphous solid (65 mg, 42 % yield). Isolated as a white amorphous solid, a single spot by TLC. UV-active and stains green with PMA; ¹H NMR (400 MHz, CDCl₃) δ 8.33–8.28 (m, 1H), 7.99–7.95 (m, 2H), 7.41–7.31 (m, 3H), 4.43 (dd, *J* = 11.6, 1.7 Hz, 1H), 4.31 (ddd, *J* = 10.8, 5.7, 2.6 Hz, 1H), 4.03 (dd, *J* = 14.1, 7.3 Hz, 1H), 3.91–3.85 (m, 2H), 3.75 (dd, *J* = 14.1, 5.5 Hz, 1H), 3.71 (d, *J* = 4.3 Hz, 1H), 3.64 (s, 1H), 3.43 (dd, *J* = 10.6, 5.0 Hz, 1H), 3.40–3.35 (m, 1H), 3.33 (s, 3H), 2.59 (dq, *J* = 10.0, 6.8 Hz, 1H), 2.35–1.16 (m, 23H), 1.53 (s, 3H), 1.13 (d, *J* = 6.8 Hz, 3H), 1.02 (d, *J* = 6.9 Hz, 3H), 0.94 (d, *J* = 6.6 Hz, 3H), 0.88 (d, *J* = 7.2 Hz, 3H), 0.85 (d, *J* = 7.1 Hz, 3H), 0.80 (d, *J* = 6.2 Hz, 3H), 0.65 (t, *J* = 7.5 Hz, 3H) ppm; ¹³C{¹H} NMR (101 MHz, CDCl₃) δ 184.2, 166.9, 134.6, 130.8, 128.2, 127.4, 107.7, 96.9, 86.3, 85.1, 85.0, 82.9, 82.1, 77.6, 74.5, 70.8, 65.9, 57.8, 47.5, 44.2, 39.2, 38.7, 36.8, 35.8, 35.3, 34.2, 33.9, 33.3, 32.6, 30.4, 29.8, 28.0, 26.6, 17.4, 16.6, 16.3, 15.6, 10.2, 9.9, 8.0 ppm; HRMS (ESI) *m/z*: [M]⁺ Calcd for C₄₃H₆₇NNaO₁₁ 796.4606; Found 796.4595.

4.2.4. Synthesis of C26-phenyl urea of MON (compound 4)

MON amine (compound 2, 152 mg, 0.23 mmol, 1.0 equiv.) was dissolved in anhydrous toluene (10 mL). Phenyl isocyanate (27 mg, 0.23 mmol, 1.0 equiv.) was added dropwise to the reaction mixture. After 72 h, the reaction mixture was concentrated on a rotary evaporator *in vacuo*. Purification on silica gel using the CombiFlash system (0 %→100 % EtOAc/hexane) gave the pure urea 4 as a clear oil. After twice evaporation to dryness with *n*-pentane, the oily product was completely converted into white amorphous solid (107 mg, 60 % yield). Isolated as a white amorphous solid, a single spot by TLC. UV-active and stains green with PMA; ¹H NMR (401 MHz, CDCl₃) δ 8.31–8.25 (m, 1H), 8.19 (s, 1H), 7.48 (dd, *J* = 8.7, 1.1 Hz, 2H), 7.18–7.12 (m, 2H), 6.86–6.80 (m, 1H), 4.34–4.25 (m, 2H), 3.89 (s, 1H), 3.85–3.81 (m, 2H), 3.76 (dd, *J* = 13.9, 9.7 Hz, 1H), 3.57 (s, 1H), 3.37 (t, *J* = 5.3 Hz, 1H), 3.35 (s, 3H), 3.29 (dd, *J* = 10.2, 2.6 Hz, 1H), 3.22 (dd, *J* = 13.9, 3.1 Hz, 1H), 2.67–2.59 (m, 1H), 2.36 (td, *J* = 11.5, 6.5 Hz, 1H), 2.28–2.18 (m, 2H), 2.15–1.22 (m, 20H), 1.55 (s, 3H), 1.21 (d, *J* = 6.8 Hz, 3H), 1.13 (d, *J* = 6.9 Hz, 3H), 0.95–0.89 (m, 6H), 0.85–0.80 (m, 6H), 0.50 (t, *J* = 7.4 Hz, 3H) ppm; ¹³C{¹H} NMR (101 MHz, CDCl₃) δ 183.5, 157.1, 140.5, 128.3, 120.9, 117.8, 107.4, 97.0, 86.5, 85.5, 85.1, 83.2, 82.3, 77.4, 75.1, 70.6, 66.5, 57.8, 47.4, 44.5, 38.7, 38.3, 36.3, 36.2, 35.3, 34.2, 33.8, 33.2,

32.4, 32.3, 30.0, 29.8, 27.9, 26.9, 17.3, 16.6, 16.5, 15.6, 10.2, 10.1, 7.8 ppm; HRMS (ESI) *m/z*: [M]⁺ Calcd for C₄₃H₆₈N₂NaO₁₁ 811.4715; Found 811.4703.

4.2.5. Synthesis of C26-amide-conjugate of MON with TPP⁺ (compound 5)

(3-carboxypropyl)triphenylphosphonium bromide (213 mg, 0.50 mmol, 1.0 equiv.) was dissolved in anhydrous DMF (15 mL) and the solution was cooled to –5 °C. Ethyl chloroformate (48 mg, 0.45 mmol, 0.9 equiv.) and triethylamine (75 mg, 0.74 mmol, 1.5 equiv.) were added dropwise. After 30 min the solution of MON amine (compound 2, 400 mg, 0.60 mmol, 1.2 equiv.) in anhydrous DMF was added dropwise. The mixture was allowed to warm to ambient temperature. After 24 h, the reaction mixture was concentrated on a rotary evaporator. The oily residue was dissolved in a small amount of CH₂Cl₂ and extracted with brine. Organic phases were concentrated under reduced pressure. Purification on silica gel using the CombiFlash system (0 → 30 % MeOH/chloroform) gave the pure product as a clear oil. The oil was diluted in *n*-pentane and evaporated to dryness three times to form an amorphous solid, with an isolated yield of 43 % (230 mg), a single spot by TLC. UV-active and stains green with PMA; ¹H NMR (401 MHz, CD₃OD) δ 7.93–7.87 (m, 3H), 7.83 (tt, *J* = 5.4, 1.3 Hz, 4H), 7.81–7.73 (m, 8H), 4.16 (dt, *J* = 8.7, 6.7 Hz, 1H), 4.10 (dd, *J* = 8.7, 2.3 Hz, 1H), 3.91 (d, *J* = 4.6 Hz, 1H), 3.73–3.65 (m, 2H), 3.62–3.59 (m, 1H), 3.54–3.47 (m, 2H), 3.46–3.39 (m, 2H), 3.35 (s, 3H), 3.30 (p, *J* = 3.3, 1.6 Hz, 2H), 3.22 (d, *J* = 13.5 Hz, 1H), 2.60–2.53 (m, 3H), 2.28–1.35 (m, 25H), 1.33 (s, 3H), 1.13 (d, *J* = 7.0 Hz, 3H), 1.03–0.89 (m, 18H) ppm; ¹³C{¹H} NMR (101 MHz, CD₃OD) δ 179.1, 174.1, 136.5, 136.4, 134.9, 134.8, 131.7, 131.6, 120.2, 119.3, 108.9, 98.5, 88.9, 87.9, 86.9, 85.0, 83.5, 79.8, 78.1, 72.8, 69.1, 59.0, 42.1, 40.3, 38.6, 38.2, 37.8, 36.8, 36.4, 36.3, 36.2, 36.1, 35.4, 32.9, 32.5, 30.6, 29.2, 26.2, 20.02, 19.99, 18.3, 16.7, 16.5, 12.9, 12.4, 11.5, 8.5 ppm; ³¹P NMR (162 MHz, CD₃OD) δ 23.5 ppm; HRMS (ESI) *m/z*: [M]⁺ Calcd for C₅₈H₈₃NO₁₁P⁺ 1000.5698; Found 1000.5732.

4.2.6. Synthesis of C1-ester-conjugate of MON with TPP⁺ (compound 6)

MON (1.0 g, 1.49 mmol, 1.0 equiv.) was dissolved in toluene (30 mL) and the solution was heated to 90 °C on a heating mantle. After 15 min DBU (386 mg, 2.53 mmol, 1.7 equiv.) was added dropwise to the reaction mixture, and after another 20 min 1,4-dibromobutane (965 mg, 4.47 mmol, 3.0 equiv.) was added dropwise. The solution changed its color to brownish after a few minutes. After 24 h, the reaction mixture was concentrated on a rotary evaporator. Purification on silica gel using the CombiFlash system (0 %→50 % EtOAc/hexane) gave the pure ester as a clear oil. After twice evaporation to dryness with *n*-pentane, the product remained in an oily form (700 mg, 58 % yield). This compound (400 mg, 0.50 mmol, 1.0 equiv.) was then dissolved in CH₃CN (30 mL) and the triphenylphosphine (1.50 mmol, 3.0 equiv., 393 mg) was added. The solution was heated under reflux on a heating mantle for 72 h. After this time, the reaction mixture was concentrated on a rotary evaporator. Purification on silica gel using the CombiFlash system (0 % → 40 % acetone/CHCl₃) gave compound 6 as clear oil. After twice evaporation to dryness with *n*-pentane, the oily products were completely converted into white amorphous solid (74 mg, 14 % yield). Isolated as a white amorphous solid, a single spot by TLC. UV-active and stains green with PMA; ¹H NMR (400 MHz, CD₃CN) δ 7.91–7.84 (m, 3H), 7.83–7.76 (m, 6H), 7.76–7.69 (m, 6H), 5.78 (d, *J* = 1.3 Hz, 1H), 5.53–5.50 (m, 1H), 4.37 (ddd, *J* = 9.5, 7.2, 4.1 Hz, 1H), 4.19–4.07 (m, 4H), 4.06 (d, *J* = 3.5 Hz, 2H), 4.02–3.94 (m, 2H), 3.82 (dt, *J* = 5.4, 2.6 Hz, 1H), 3.69 (dd, *J* = 5.3, 2.9 Hz, 1H), 3.67–3.55 (m, 4H), 3.51–3.41 (m, 2H), 3.38 (ddd, *J* = 10.1, 4.0, 1.7 Hz, 2H), 3.19 (s, 3H), 2.83 (ddd, *J* = 13.8, 6.8, 2.8 Hz, 1H), 2.60 (s, 1H), 2.34 (s, 1H), 2.31–2.23 (m, 3H), 2.18–1.26 (m, 13H), 1.47 (s, 3H), 1.19 (s, 2H), 1.10 (d, *J* = 6.9 Hz, 3H), 0.98 (d, *J* = 7.0 Hz, 3H), 0.93–0.84 (m, 9H), 0.75 (d, *J* = 6.8 Hz, 3H), 0.72 (d, *J* = 7.1 Hz, 3H) ppm; ¹³C{¹H} NMR (101 MHz, CD₃CN) δ 176.0, 135.8, 135.8, 134.6, 134.5, 131.1, 131.0, 119.6, 118.7, 108.4, 99.0, 86.6, 86.4, 84.6, 81.8, 81.6, 76.3, 74.7, 69.6, 69.1, 67.0, 63.8, 58.4, 55.2, 41.3, 39.9, 36.8, 36.5, 36.3, 35.5, 35.1, 34.6, 33.4, 33.2, 32.2, 30.4, 30.1, 30.0,

29.7, 29.6, 28.3, 26.8, 22.6, 22.1, 20.0, 20.0, 16.4, 16.1, 14.5, 13.2, 11.5, 10.8, 8.1 ppm; ^{31}P NMR (162 MHz, CN_3CN) δ 25.2 ppm; HRMS (ESI) m/z : $[\text{M}]^+$ Calcd for $\text{C}_{58}\text{H}_{84}\text{O}_{11}\text{P}^+$ 987.5746; Found 987.5745.

4.2.7. Synthesis of C1-benzyl ester of MON (compound 7)

MON (0.5 g, 0.75 mmol, 1.0 equiv.) was dissolved in toluene (20 mL) and the solution was heated to 90 °C on a heating mantle. After 15 min DBU (193 mg, 1.27 mmol, 1.7 equiv.) was added dropwise to the reaction mixture, and after another 20 min benzyl bromide (382 mg, 2.24 mmol, 3.0 equiv.) was added dropwise. The solution changed its color to brownish after a few minutes. After 24 h, the reaction mixture was concentrated on a rotary evaporator *in vacuo*. Purification on silica gel using the CombiFlash system (0 %→50 % EtOAc/hexane) gave the pure ester 7 as a clear oil. After twice evaporation to dryness with *n*-pentane, the oily product was completely converted into white amorphous solid (438 mg, 77 % yield). Isolated as a white amorphous solid, a single spot by TLC. UV-active and stains green with PMA; ^1H NMR (401 MHz, CDCl_3) δ 7.39–7.27 (m, 5H), 5.19 (d, J = 12.4 Hz, 1H), 5.12 (d, J = 12.4 Hz, 1H), 4.37 (d, J = 9.3 Hz, 1H), 4.27 (td, J = 8.0, 3.3 Hz, 1H), 4.04 (dd, J = 9.1, 2.3 Hz, 1H), 3.87 (s, 1H), 3.84 (d, J = 4.7 Hz, 1H), 3.81–3.72 (m, 2H), 3.61–3.56 (m, 2H), 3.47–3.43 (m, 2H), 3.23 (s, 3H), 2.70 (ddd, J = 13.8, 6.9, 3.9 Hz, 2H), 2.31–2.23 (m, 1H), 2.18–1.30 (m, 20H), 1.35 (s, 3H), 1.20 (d, J = 7.0 Hz, 3H), 0.98 (d, J = 6.9 Hz, 3H), 0.95 (d, J = 7.0 Hz, 3H), 0.89 (t, J = 7.4 Hz, 3H), 0.87–0.81 (m, 9H) ppm; $^{13}\text{C}\{^1\text{H}\}$ NMR (101 MHz, CDCl_3) δ 175.2, 136.1, 128.4, 128.2, 128.0, 107.5, 96.8, 87.2, 86.2, 85.6, 83.5, 81.4, 76.4, 76.3, 71.2, 68.0, 67.4, 66.2, 58.1, 40.9, 39.0, 37.0, 36.7, 36.0, 35.1, 34.7, 34.4, 33.5, 32.7, 32.2, 31.0, 29.5, 27.8, 25.6, 17.3, 16.0, 15.6, 12.2, 11.6, 11.0, 6.0 ppm; HRMS (ESI) m/z : $[\text{M} + \text{Na}]^+$ Calcd for $\text{C}_{43}\text{H}_{68}\text{NaO}_{11}$ 783.4654; Found 783.4661.

4.2.8. Synthesis of C26-phenyl O-urethane of MON (compound 8)

MON (compound 1, 200 mg, 0.30 mmol, 1.0 equiv.) was dissolved in anhydrous toluene (10 mL). Phenyl isocyanate (34 mg, 0.28 mmol, 0.95 equiv.) was added dropwise to the reaction mixture. After 2 weeks, the reaction mixture was concentrated on a rotary evaporator *in vacuo*. Purification on silica gel using the CombiFlash system (0 %→50 % EtOAc/hexane) gave the pure urethane 8 as a clear oil. After twice evaporation to dryness with *n*-pentane, the oily product was completely converted into white amorphous solid (127 mg, 54 % yield). Isolated as a white amorphous solid, a single spot by TLC. UV-active and stains green with PMA; ^1H NMR (401 MHz, CD_3CN) δ 7.94 (s, 1H), 7.48–7.41 (m, 2H), 7.31–7.25 (m, 2H), 7.06–6.99 (m, 1H), 4.24–4.17 (m, 2H), 4.09 (dd, J = 10.1, 1.5 Hz, 1H), 4.02 (d, J = 11.4 Hz, 1H), 3.93 (d, J = 4.2 Hz, 1H), 3.76 (dd, J = 9.7, 2.9 Hz, 1H), 3.67 (s, 1H), 3.57 (dd, J = 10.0, 5.2 Hz, 1H), 3.41–3.37 (m, 1H), 3.33 (s, 3H), 2.58 (p, J = 6.8 Hz, 1H), 2.19–1.27 (m, 24H), 1.39 (s, 3H), 1.15 (d, J = 6.8 Hz, 3H), 1.02 (d, J = 6.9 Hz, 3H), 0.90 (d, J = 3.8 Hz, 3H), 0.89 (d, J = 4.2 Hz, 3H), 0.87–0.81 (m, 9H) ppm; $^{13}\text{C}\{^1\text{H}\}$ NMR (101 MHz, CD_3CN) δ 177.4, 154.7, 139.9, 129.9, 123.9, 120.1, 119.6, 108.8, 97.7, 87.5, 87.4, 86.2, 84.3, 82.6, 78.0, 77.0, 72.1, 68.3, 68.2, 58.6, 41.5, 39.7, 37.8, 37.4, 36.7, 35.8, 35.4, 35.3, 34.1, 33.8, 33.4, 31.9, 31.0, 28.7, 27.1, 18.0, 16.7, 16.3, 14.0, 12.0, 11.3, 8.7 ppm; HRMS (ESI) (m/z): $[\text{M} + \text{Na}]^+$ Calcd for $\text{C}_{43}\text{H}_{67}\text{NNaO}_{12}$ 812.4555; found 812.4573.

4.3. X-ray measurements

The X-ray intensity data for compounds 4, and 5 were collected using graphite monochromatic Mo K_α radiation on a four-circle κ geometry Xcalibur diffractometer with Sapphire2 area CCD detector. Data collections were made using the CrysAlisPro 1.171.42.93a. Integration, scaling of the reflections, corrections for Lorenz and polarization effects and absorption corrections were performed using the CrysAlisPro 1.171.42.93a program.²⁸ Using Olex2,²⁹ the structure was solved by the direct methods using SHELXT-2014/5³⁰ and refined using SHELXL-2018/3 program.³¹ The hydrogen atoms joined to carbon atoms were

introduced in their geometrical positions and treated as rigid. The H atoms involved in the hydrogen bonds were refined if they gave reasonable hydrogen bonds, otherwise they were constrained. It was not possible to locate all solvent molecules in crystal 4 due to their high disorder. Since it was not possible to correctly model the disordered molecules, we performed a “squeeze” treatment to remove the contribution of these molecules to the scattering. The final difference Fourier maps showed no peaks of chemical significance. Details of the data collection parameters, crystallographic data and final agreement parameters are collected in Table S1. The hydrogen bonds are summarized in Tables S2–S3. Visualizations of the structures were made with the Diamond 3.0.³²

4.4. In vitro assessment of hepatic stage antiplasmodial activity

The compounds' antiplasmodial activity was assessed *in vitro* in Huh7 cells, a human hepatoma cell line provided by Cenix Bioscience GmbH and maintained in complete culture medium, consisting of Roswell Park Memorial Institute (RPMI) 1640 medium supplemented with 10 % (v/v) fetal bovine serum (FBS), 1 % (v/v) penicillin/streptomycin, 1 % (v/v) glutamine, 1 % (v/v) non-essential amino acids, and 10 mM 2-(4-(2-hydroxyethyl)piperazine-1-yl) ethanesulfonic acid (HEPES) pH 7 (all from Gibco).

Stock solutions of the test compounds (10 mM) were prepared in dimethyl sulfoxide (DMSO) and serially diluted in infection medium – complete RPMI 1640 supplemented with 0.8 $\mu\text{g}/\text{mL}$ amphotericin B and 50 $\mu\text{g}/\text{mL}$ gentamicin (both from Thermo Fisher Scientific) – to achieve the desired test concentrations. Huh7 cells were seeded at a density of 1×10^4 cells per well in 96-well plates and incubated at 37 °C with 5 % CO_2 and humidified atmosphere for 24 h. After incubation, the culture medium was removed, and the test compounds, diluted in infection medium, were added to the cells in triplicate. The cells were incubated with the compounds for 1 h at 37 °C with 5 % CO_2 and humidified atmosphere. DMSO and Primaquine were used as the negative and positive controls, respectively. Cells were then infected with 1×10^4 luciferase-expressing *P. berghei* sporozoites, freshly extracted from the salivary glands of infected female *Anopheles stephensi* mosquitoes reared in the GiMM insectarium. The plates were centrifuged at $1800 \times g$ for 5 min at room temperature and then incubated at 37 °C with 5 % CO_2 and humidified atmosphere. Cell viability was assessed 46 h later using the AlamarBlue assay, according to the manufacturer's instructions (Invitrogen). Parasite burden was determined 48 h after sporozoite infection by a bioluminescence assay (Biotium). Fluorescence and bioluminescence were measured with a microplate reader (Tecan Spark). IC_{50} values were calculated using GraphPad Prism software through nonlinear regression analysis of normalized dose–response curves.

4.5. In vitro assessment of compounds cytotoxicity

The cytotoxicity of the test compounds to Huh7 cells was assessed under similar conditions to those described above. Briefly, cells were seeded in 96-well plates at 1×10^4 cells per well and incubated in complete RPMI at 37 °C with 5 % CO_2 and humidified atmosphere for 24 h. The culture medium was then replaced with compound-containing complete medium, supplemented with 0.8 $\mu\text{g}/\text{mL}$ amphotericin B and 50 $\mu\text{g}/\text{mL}$ gentamicin, at the desired test concentrations. DMSO in amounts equivalent to those present in the different compound dilutions was used as a negative control. After a 46 h incubation, cell viability was assessed using the AlamarBlue assay, and fluorescence was measured using a microplate reader. CC_{50} values were determined by nonlinear regression analysis of normalized dose–response curves using GraphPad Prism software.

CRedit authorship contribution statement

Michał Sulik: Writing – review & editing, Writing – original draft,

Methodology, Investigation, Data curation, Conceptualization. **Eyob A. Workneh:** Writing – original draft, Methodology, Investigation, Data curation, Conceptualization. **Sofia Santana:** Investigation. **Bárbara Teixeira:** Methodology, Investigation. **Miguel Prudêncio:** Writing – original draft, Validation, Methodology, Conceptualization. **Jan Janczak:** Writing – original draft, Visualization, Validation, Software, Investigation, Data curation. **Adam Huczyński:** Writing – review & editing, Writing – original draft, Validation, Supervision, Resources, Project administration, Funding acquisition, Formal analysis, Conceptualization.

Declaration of competing interest

The authors declare that they have no known competing financial interests or personal relationships that could have appeared to influence the work reported in this paper.

Acknowledgements

This research was financially supported by an OPUS 21 grant (2021/41/B/ST4/00088) funded to A.H. by the National Science Center in Poland (NCN). For the purpose of Open Access, the authors have applied public copyright license to any Author Accepted Manuscript (AAM) version arising from this submission. M.S. wishes to acknowledge the Adam Mickiewicz University Foundation for a scholarship for the academic year 2024/2025. M.P. is grateful for support from “la Caixa” Foundation’s grant HR-848 and European Union Horizon Europe programme’s grant 101080744. The graphical abstract was created with BioRender.com, accessed on 22 January 2025.

Appendix A. Supplementary data

Supplementary data to this article can be found online at <https://doi.org/10.1016/j.bmc.2025.118177>.

Data availability

Data will be made available on request.

References

- World Health Organization – World Malaria Report 2024 (on-line access: 2025-01-23). <https://www.who.int/teams/global-malaria-programme/reports/world-malaria-report-2024>.
- Phillips MA, Burrows JN, Manyando C, van Huijsdijnen RH, Van Voorhis WC, Malaria WTNC. *Nat Rev Dis Primers*. 2017;3:17050. <https://doi.org/10.1038/nrdp.2017.50>.
- Centers for Disease Control and Prevention – Malaria (on-line access: 2025-01-23). <https://www.cdc.gov/malaria/index.html>.
- Prudêncio M, Rodriguez A, Mota MM. The Silent Path to Thousands of Merozoites: The Plasmodium Liver Stage. *Nat Rev Microbiol*. 2006;4:849–856. <https://doi.org/10.1038/nrmicro1529>.
- Duffy PE, Patrick GJ. Malaria Vaccines since 2000: Progress, Priorities, Products. *npj Vaccines*. 2020;5:48. <https://doi.org/10.1038/s41541-020-0196-3>.
- White NJ. Antimalarial Drug Resistance. *J Clin Invest*. 2004;113:1084–1092. <https://doi.org/10.1172/JCI21682>.
- Antoszczak M, Steverding D, Huczyński A. Anti-Parasitic Activity of Polyether Ionophores. *Eur J Med Chem*. 2019;166:32–47. <https://doi.org/10.1016/j.ejmech.2019.01.035>.
- Taborda CP, Travassos LR. Peptide Vaccine Against Paracoccidiodomycosis. In: *Vaccines for Invasive Fungal Infections. Methods in Molecular Biology*. New York, NY: Humana Press; 2017:113–128. https://doi.org/10.1007/978-1-4939-7104-6_9.
- Antoszczak M, Rutkowski J, Huczyński A. Structure and Biological Activity of Polyether Ionophores and Their Semisynthetic Derivatives. In: *Bioactive Natural Products*. Wiley; 2014:107–170. <https://doi.org/10.1002/9783527684403.ch6>.
- Steverding D, Antoszczak M, Huczyński A. In Vitro Activity of Salinomycin and Monensin Derivatives against Trypanosoma Brucei. *Parasit Vectors*. 2016;9:409. <https://doi.org/10.1186/s13071-016-1698-8>.
- Osorio Y, Travi BL, Renslo AR, Peniche AG, Melby P. C. Identification of Small Molecule Lead Compounds for Visceral Leishmaniasis Using a Novel Ex Vivo Splenic Explant Model System. *PLoS Negl Trop Dis*. 2011;5:e962.
- Couzinet S, Dubremetz JF, Buzoni-Gatel D, Jeminet G, Prensier G. In Vitro Activity of the Polyether Ionophorous Antibiotic Monensin against the Cyst Form of Toxoplasma Gondii. *Parasitology*. 2000;121:359–365. <https://doi.org/10.1017/S0031182099006605>.
- Rochdi M, Delort A-M, Guyot J, et al. Ionophore Properties of Monensin Derivatives Studied on Human Erythrocytes by ²³Na NMR and K⁺ and H⁺ Potentiometry: Relationship with Antimicrobial and Antimalarial Activities. *J Med Chem*. 1996;39:588–595. <https://doi.org/10.1021/jm9505829>.
- Tanaka R, Nagatsu A, Mizukami H, Ogihara Y, Sakakibara J. Studies on Chemical Modification of Monensin. IX. Synthesis of 26-Substituted Monensins and Their Na⁺-Ion Transport Activity. *Chem Pharm Bull (Tokyo)*. 2001;49:711–715. <https://doi.org/10.1248/cpb.49.711>.
- Lowicki D, Huczyński A. Structure and Antimicrobial Properties of Monensin A and Its Derivatives: Summary of the Achievements. *Biomed Res Int*. 2013;2013:1–14. <https://doi.org/10.1155/2013/742149>.
- Klejborowska G, Jędrzejczyk M, Stepczyńska N, Maj E, Wietrzyk J, Huczyński A. Antiproliferative Activity of Ester Derivatives of Monensin A at the C-1 and C-26 Positions. *Chem Biol Drug Des*. 2019;94:1859–1864. <https://doi.org/10.1111/cbdd.13581>.
- Jędrzejczyk M, Stepczyńska N, Klejborowska G, et al. Synthesis and Evaluation of Antibacterial and Trypanocidal Activity of Derivatives of Monensin A. *Bioorg Med Chem Lett*. 2022;58, 128521. <https://doi.org/10.1016/j.bmcl.2021.128521>.
- Westley JW, Liu C-M, Evans Jr RH, Sello LH, Troupe N, Hermann T. Preparation, Properties and Biological Activity of Natural and Semisynthetic Urethanes of Monensin. *J Antibiot (Tokyo)*. 1983;36:1195–1200. <https://doi.org/10.7164/antibiotics.36.1195>.
- Delaveau J, Vialle E, Lemaire M., Pellet-Rostaing S., Andrioletti B. Novel Monensin Derivatives for the Treatment and Prevention of Protozoal Infections, 2016 patent no. HUE031125T2.
- Huczyński A, Janczak J, Lowicki D, Brzezinski B. Monensin A Acid Complexes as a Model of Electrogenic Transport of Sodium Cation. *Biochim Biophys Acta – Biomembr*. 2012;1818:2108–2119. <https://doi.org/10.1016/j.bbamem.2012.04.017>.
- Antonenko YN, Rokitskaya TI, Huczyński A. Electrogenic and Nonelectrogenic Ion Fluxes across Lipid and Mitochondrial Membranes Mediated by Monensin and Monensin Ethyl Ester. *Biochim Biophys Acta – Biomembr*. 2015;1848:995–1004. <https://doi.org/10.1016/j.bbamem.2015.01.005>.
- Sulik M, Graniczny R, Janczak J, Kłopotowska D, Wietrzyk J, Huczyński A. From Pseudocyclic to Macrocyclic Ionophores: Strategies toward the Synthesis of Cyclic Monensin Derivatives. *J Org Chem*. 2025. <https://doi.org/10.1021/acs.joc.4c02715>.
- Pourahmad J, Salimi A, Seydi E. Mitochondrial Targeting for Drug Development. In: *Toxicology Studies – Cells, Drugs and Environment*. InTech; 2015. <https://doi.org/10.5772/59719>.
- Battogtokh G, Choi YS, Kang DS, et al. Mitochondria-Targeting Drug Conjugates for Cytotoxic, Anti-Oxidizing and Sensing Purposes: Current Strategies and Future Perspectives. *Acta Pharm Sin B*. 2018;8:862–880. <https://doi.org/10.1016/j.apsb.2018.05.006>.
- Goodman CD, Buchanan HD, McFadden GI. Is the Mitochondrion a Good Malaria Drug Target? *Trends Parasitol*. 2017;33:185–193. <https://doi.org/10.1016/j.pt.2016.10.002>.
- Hikosaka K, Komatsuya K, Suzuki S, Kita K. Mitochondria of Malaria Parasites as a Drug Target. In: *An Overview of Tropical Diseases*. InTech; 2015. <https://doi.org/10.5772/61283>.
- Huczyński A, Ratajczak-Sitarz M, Stefańska J, Katrusiak A, Brzezinski B, Bartl F. Reinvestigation of the Structure of Monensin A Phenylurethane Sodium Salt Based on X-Ray Crystallographic and Spectroscopic Studies, and Its Activity against Hospital Strains of Methicillin-Resistant S Epidermidis and s. Aureus. *J Antibiot (Tokyo)*. 2011;64:249–256. <https://doi.org/10.1038/ja.2010.167>.
- Rigaku Oxford Diffraction, CrysAlisPro 1.171.42.93a Software system, Oxford, UK, 2023. <https://rigaku.com/products/crystallography/x-ray-diffraction/crystalpro>.
- Dolomanov OV, Bourhis LJ, Gildea RJ, Howard RJ, Puschmann H. OLEX2: A Complete Structure Solution, Refinement and Analysis Program. *J Appl Cryst*. 2009;42:339–341. <https://doi.org/10.1107/S0021889808042726>.
- Sheldrick GM. SHELXT – Integrated Space-Group and Crystal-Structure Determination. *Acta Crystallogr A Found Adv*. 2015;71:3–8. <https://doi.org/10.1107/S2053273314026370>.
- Sheldrick GM. Crystal Structure Refinement with SHELXL. *Acta Crystallogr C Struct Chem*. 2015;71:3–8. <https://doi.org/10.1107/S2053229614024218>.
- Putz H., Brandenburg K. DIAMOND Version 3.0, Crystal Impact GbR, Bonn, Germany, 2014.